

Fig. 1: Comparisons of deraining methods working on LFIs. The de-rained central sub-view generated by each method is scored with the PSNR/SSIM. The best value is highlighted with **bold**, and the second-best value is colored with **cyan**.



Fig. 2: Comparisons of deraining methods working on LFIs. The de-rained central sub-view generated by each method is scored with the PSNR/SSIM. The best value is highlighted with **bold**, and the second-best value is colored with **cyan**.



Fig. 3: Comparisons of deraining methods working on LFIs. The de-rained central sub-view generated by each method is scored with the PSNR/SSIM. The best value is highlighted with **bold**, and the second-best value is colored with **cyan**.



Fig. 4: Comparisons of deraining methods working on LFIs. The de-rained central sub-view generated by each method is scored with the PSNR/SSIM. The best value is highlighted with **bold**, and the second-best value is colored with **cyan**.

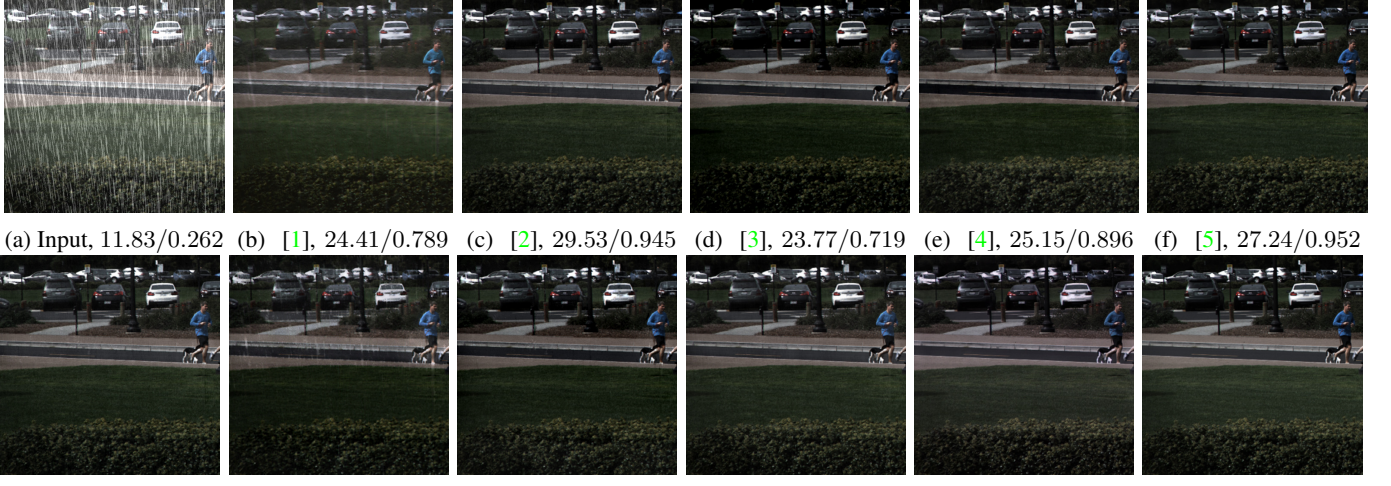


Fig. 5: Comparisons of deraining methods working on synthetic LFIs. The de-rained central sub-view generated by each method is scored with the PSNR/SSIM. The best value is highlighted with **bold**, and the second-best value is colored with **cyan**.



Fig. 6: Comparisons of deraining methods working on synthetic LFIs. The de-rained central sub-view generated by each method is scored with the PSNR/SSIM. The best value is highlighted with **bold**, and the second-best value is colored with **cyan**.

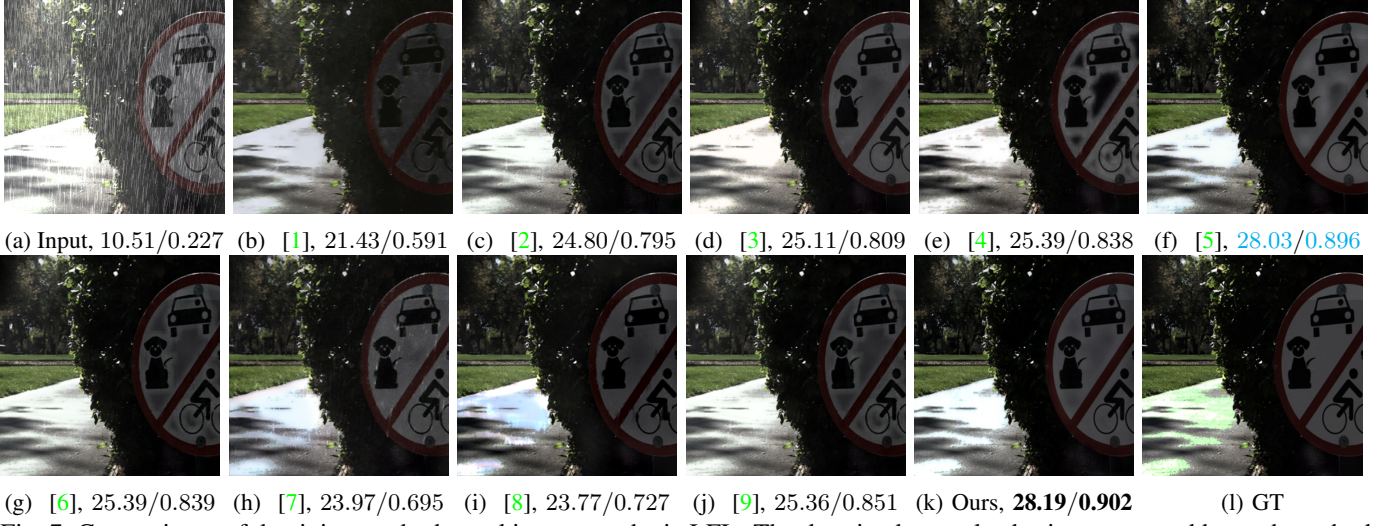


Fig. 7: Comparisons of deraining methods working on synthetic LFIs. The de-rained central sub-view generated by each method is scored with the PSNR/SSIM. The best value is highlighted with **bold**, and the second-best value is colored with **cyan**.



Fig. 8: Comparisons of deraining methods working on synthetic LFIs. The de-rained central sub-view generated by each method is scored with the PSNR/SSIM. The best value is highlighted with **bold**, and the second-best value is colored with **cyan**.



Fig. 9: Comparisons of deraining methods working on synthetic LFIs. The de-rained central sub-view generated by each method is scored with the PSNR/SSIM. The best value is highlighted with **bold**, and the second-best value is colored with **cyan**.

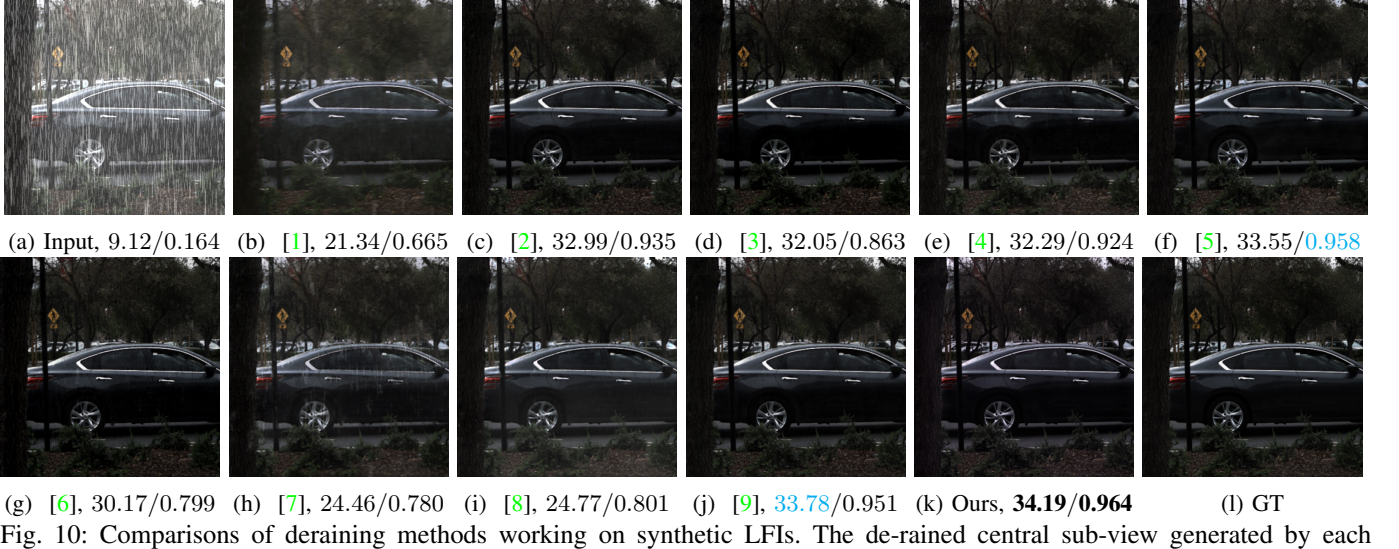


Fig. 10: Comparisons of deraining methods working on synthetic LFIs. The de-rained central sub-view generated by each method is scored with the PSNR/SSIM. The best value is highlighted with **bold**, and the second-best value is colored with **cyan**.

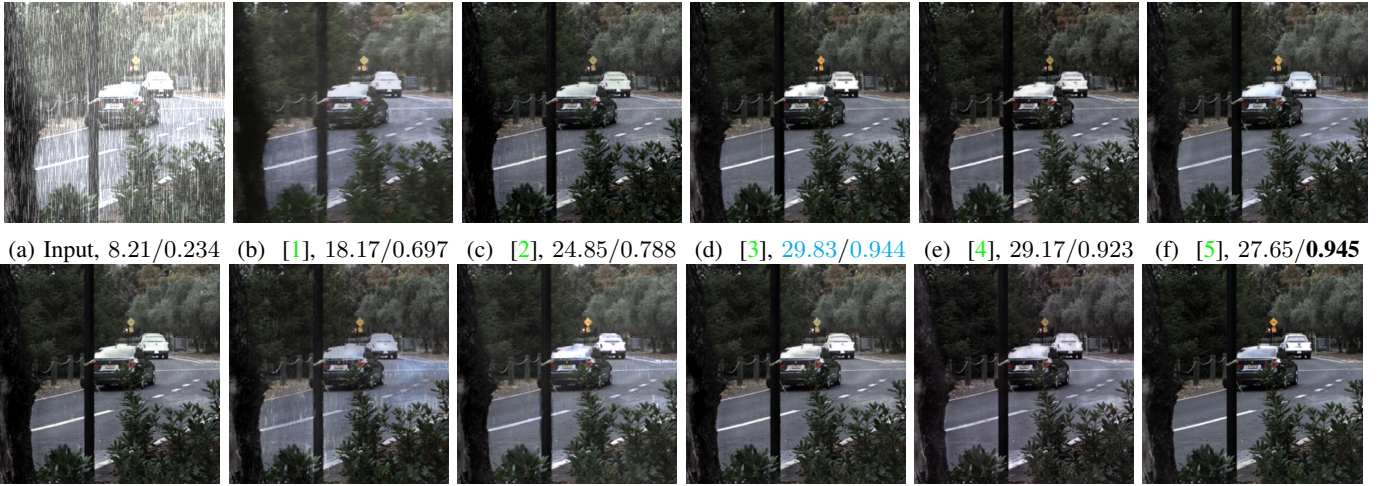


Fig. 11: Comparisons of deraining methods working on synthetic LFIs. The de-rained central sub-view generated by each method is scored with the PSNR/SSIM. The best value is highlighted with **bold**, and the second-best value is colored with **cyan**.

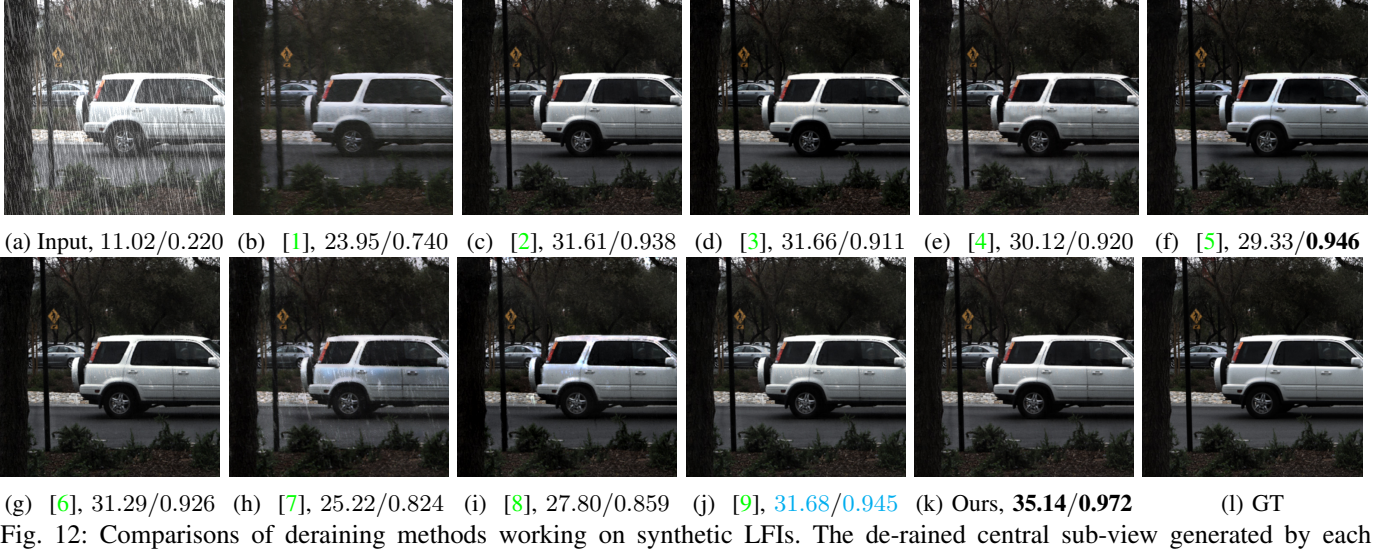


Fig. 12: Comparisons of deraining methods working on synthetic LFIIs. The de-rained central sub-view generated by each method is scored with the PSNR/SSIM. The best value is highlighted with **bold**, and the second-best value is colored with cyan.

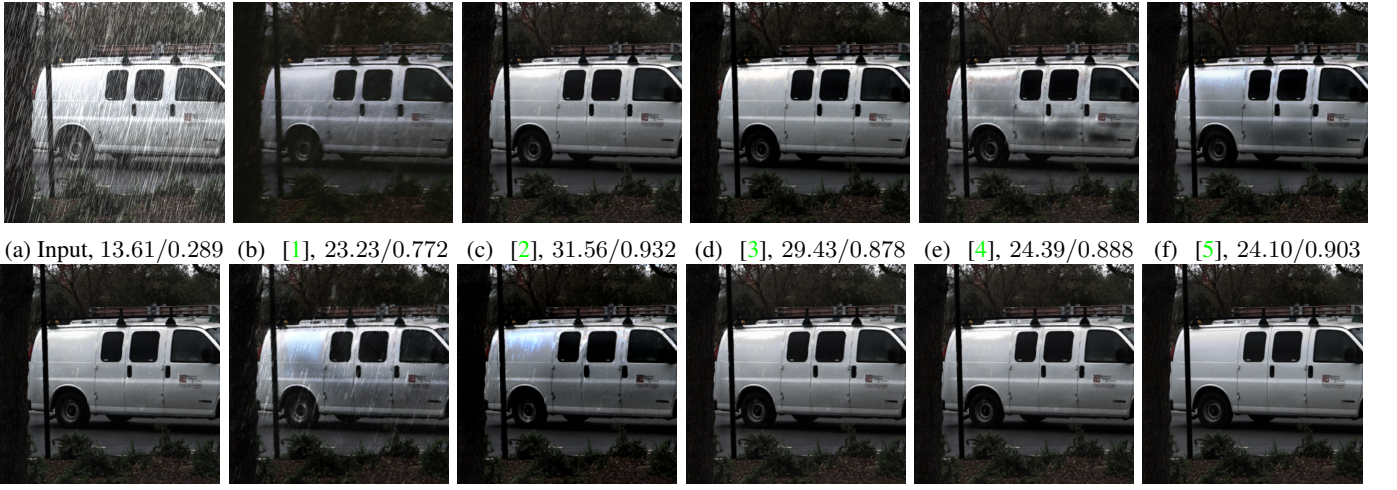
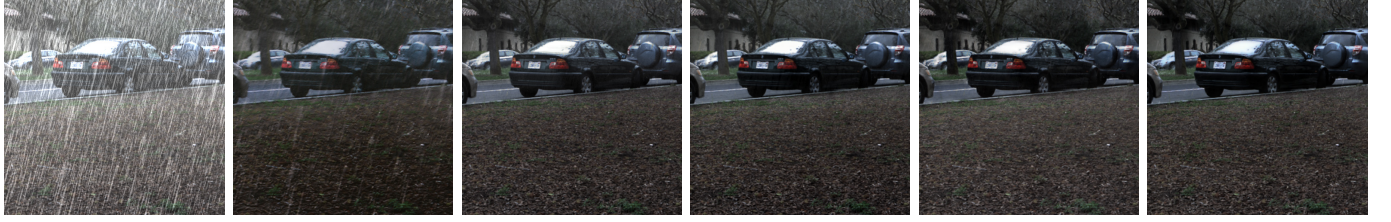


Fig. 13: Comparisons of deraining methods working on synthetic LFIIs. The de-rained central sub-view generated by each method is scored with the PSNR/SSIM. The best value is highlighted with **bold**, and the second-best value is colored with cyan.



(a) Input, 9.35/0.286 (b) [1], 22.59/0.715 (c) [2], 26.36/0.898 (d) [3], 27.37/0.924 (e) [4], 28.42/0.911 (f) [5], **32.31/0.949**



(g) [6], 25.67/0.842 (h) [7], 24.54/0.794 (i) [8], 25.78/0.872 (j) [9], 25.52/0.896 (k) Ours, **32.85/0.933** (l) GT

Fig. 14: Comparisons of deraining methods working on synthetic LFIs. The de-rained central sub-view generated by each method is scored with the PSNR/SSIM. The best value is highlighted with **bold**, and the second-best value is colored with cyan.



(a) Input, 10.06/0.186 (b) [1], 25.33/0.749 (c) [2], **32.31/0.941** (d) [3], 27.17/0.864 (e) [4], 29.71/0.904 (f) [5], 31.23/0.949



(g) [6], 31.99/0.929 (h) [7], 25.16/0.792 (i) [8], 26.68/0.833 (j) [9], 32.27/0.933 (k) Ours, **33.76/0.958** (l) GT

Fig. 15: Comparisons of deraining methods working on synthetic LFIs. The de-rained central sub-view generated by each method is scored with the PSNR/SSIM. The best value is highlighted with **bold**, and the second-best value is colored with cyan.

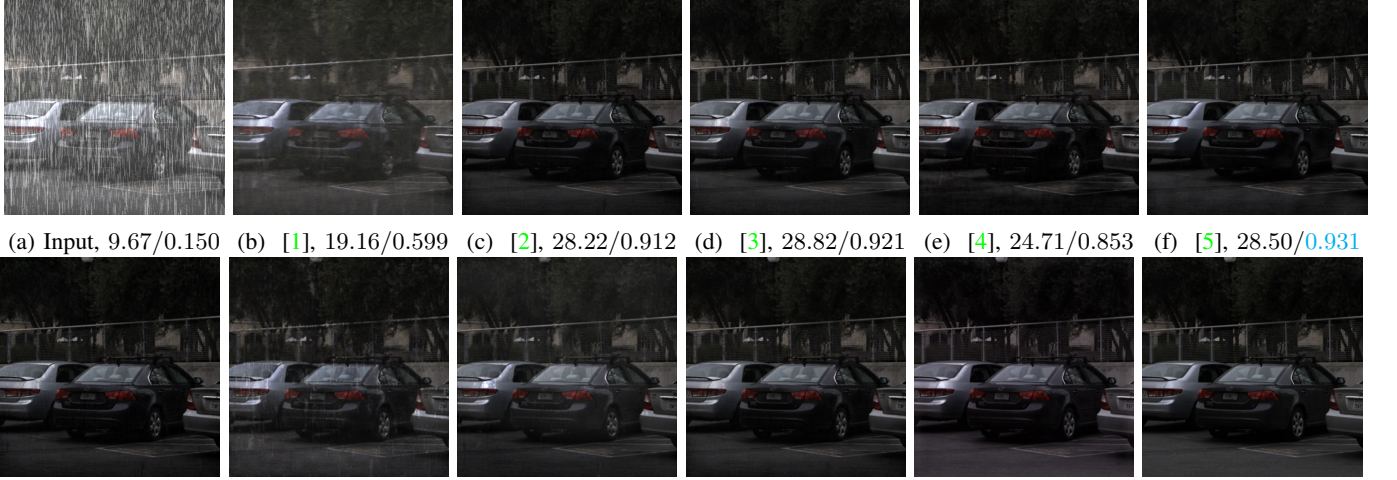


Fig. 16: Comparisons of deraining methods working on synthetic LFIs. The de-rained central sub-view generated by each method is scored with the PSNR/SSIM. The best value is highlighted with **bold**, and the second-best value is colored with cyan.



Fig. 17: Comparisons of deraining methods working on synthetic LFIs. The de-rained central sub-view generated by each method is scored with the PSNR/SSIM. The best value is highlighted with **bold**, and the second-best value is colored with cyan.



(a) Input, 10.06/0.320 (b) [1], 20.77/0.692 (c) [2], 23.89/0.863 (d) [3], 25.37/0.837 (e) [4], 27.46/0.911 (f) [5], **27.47/0.931**



(g) [6], 23.18/0.845 (h) [7], 22.95/0.763 (i) [8], 23.04/0.757 (j) [9], 24.43/0.890 (k) Ours, **28.80/0.943** (l) GT

Fig. 18: Comparisons of deraining methods working on synthetic LFIs. The de-rained central sub-view generated by each method is scored with the PSNR/SSIM. The best value is highlighted with **bold**, and the second-best value is colored with cyan.



(a) Input, 10.45/0.310 (b) [1], 23.09/0.776 (c) [2], 29.30/0.941 (d) [3], 29.14/0.933 (e) [4], 26.54/0.916 (f) [5], **26.78/0.944**



(g) [6], 28.42/0.928 (h) [7], 24.70/0.846 (i) [8], 25.56/0.909 (j) [9], **30.23/0.956** (k) Ours, **32.82/0.973** (l) GT

Fig. 19: Comparisons of deraining methods working on synthetic LFIs. The de-rained central sub-view generated by each method is scored with the PSNR/SSIM. The best value is highlighted with **bold**, and the second-best value is colored with cyan.

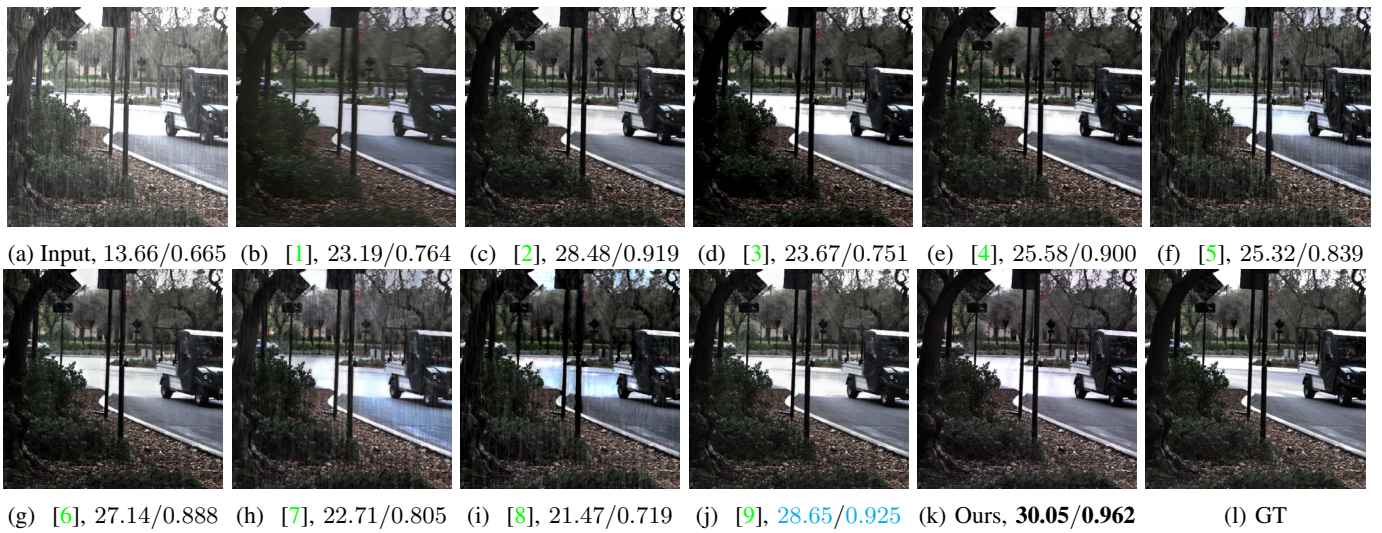


Fig. 20: Comparisons of deraining methods working on synthetic LFIs. The de-rained central sub-view generated by each method is scored with the PSNR/SSIM. The best value is highlighted with **bold**, and the second-best value is colored with **cyan**.

REFERENCES

- [1] R. Li, L. Cheong, and R. T. Tan, "Heavy rain image restoration: Integrating physics model and conditional adversarial learning," in *Proc. IEEE CVPR*, pp. 1633–1642, 2019.
- [2] W. Wei, D. Meng, Q. Zhao, Z. Xu, and Y. Wu, "Semi-supervised transfer learning for image rain removal," in *Proc. IEEE CVPR*, pp. 3877–3886, 2019.
- [3] K. Jiang, Z. Wang, P. Yi, C. Chen, Z. Han, T. Lu, B. Huang, and J. Jiang, "Decomposition makes better rain removal: An improved attention-guided deraining network," *IEEE TCSVT*, 2020.
- [4] W. Yang, R. T. Tan, J. Feng, Z. Guo, S. Yan, and J. Liu, "Joint rain detection and removal from a single image with contextualized deep networks," *IEEE TPAMI*, vol. 42, no. 6, pp. 1377–1393, 2020.
- [5] D. Ren, W. Shang, P. Zhu, Q. Hu, D. Meng, and W. Zuo, "Single image deraining using bilateral recurrent network," *IEEE TIP*, vol. 29, pp. 6852–6863, 2020.
- [6] R. Yasarla, V. A. Sindagi, and V. M. Patel, "Syn2real transfer learning for image deraining using gaussian processes," in *Proc. CVPR*, pp. 2726–2736, 2020.
- [7] S. W. Zamir, A. Arora, S. Khan, M. Hayat, F. S. Khan, M.-H. Yang, and L. Shao, "Multi-stage progressive image restoration," in *Proc. IEEE/CVF CVPR*, pp. 14821–14831, 2021.
- [8] X. Hu, L. Zhu, T. Wang, C.-W. Fu, and P.-A. Heng, "Single-image real-time rain removal based on depth-guided non-local features," *IEEE TIP*, vol. 30, pp. 1759–1770, 2021.
- [9] Y. Ding, M. Li, T. Yan, F. Zhang, Y. Liu, and R. W. Lau, "Rain streak removal from light field images," *IEEE TCSVT*, pp. 1–1, 2021.